



This article appeared in a journal published by Elsevier. The attached copy is furnished to the author for internal non-commercial research and education use, including for instruction at the authors institution and sharing with colleagues.

Other uses, including reproduction and distribution, or selling or licensing copies, or posting to personal, institutional or third party websites are prohibited.

In most cases authors are permitted to post their version of the article (e.g. in Word or Tex form) to their personal website or institutional repository. Authors requiring further information regarding Elsevier's archiving and manuscript policies are encouraged to visit:

<http://www.elsevier.com/copyright>



Contents lists available at ScienceDirect

## Journal of the Mechanics and Physics of Solids

journal homepage: [www.elsevier.com/locate/jmps](http://www.elsevier.com/locate/jmps)

## Photomechanics of light-activated polymers

Kevin N. Long<sup>a</sup>, Timothy F. Scott<sup>a</sup>, H. Jerry Qi<sup>a</sup>, Christopher N. Bowman<sup>b</sup>, Martin L. Dunn<sup>a,\*</sup><sup>a</sup> Department of Mechanical Engineering, University of Colorado at Boulder, Boulder, CO 80309, USA<sup>b</sup> Department of Chemical and Biological Engineering, University of Colorado, Boulder, CO 80309, USA

## ARTICLE INFO

## Article history:

Received 7 October 2008

Received in revised form

2 March 2009

Accepted 4 March 2009

## Keywords:

Light-activated polymers

Shape-memory polymers

Constitutive modeling

Finite deformation

Active materials

## ABSTRACT

Light-activated polymers are an exciting class of modern materials that respond mechanically when irradiated by light at particular wavelengths. While details of the mechanisms that connect the optical excitation to mechanical behavior are complex and differ from material to material, there is sufficient commonality among them to permit the development of a generalized modeling framework to describe the photomechanics. The features shared by light-activated polymers involve light interacting with the material, which triggers photochemical reactions that alter the structure of the crosslinked polymer network. Many such structural alterations result in an evolution of the polymer network, and subsequent macroscopic deformation. When this process is appropriately executed it can enable a photomechanical shape-memory effect. In this paper, we develop a three-dimensional finite-deformation modeling framework to describe the photomechanical response of light-activated polymer systems. This framework integrates four coupled phenomena that contribute to macroscopic photomechanical behavior: photophysics, photochemistry, chemomechanical coupling, and mechanical deformation. The chemomechanical coupling consists of chemically induced structural alterations of the crosslinked network that result in subsequent deformation. We describe this behavior through a decomposition of the crosslinked network into two components consisting of an original network and a photochemically altered network; both evolve during photomechanical deformation. The modeling framework presented in this paper is sufficiently general that it is applicable to light-activated polymer systems that operate with various mechanisms in each of the four areas. Using this modeling approach, we develop constitutive models for two recently developed light-activated polymer systems [Lendlein, A., Hongyan, J., Junger, O., Langer, R., 2005. Light-induced shape-memory polymers. *Nature* 434 (7035) 879; Scott, T.F., Schneider, A.D., Cook, W.D., Bowman, C.N., 2005. Photoinduced plasticity in crosslinked polymers. *Science* 308 (5728) 1615]. For the material developed by Scott and his co-workers we validate our model by measuring and numerically simulating photo-induced stress relaxation and bending deformation and obtain good agreement between measurements and predictions. Finally, we use the model to study the effects of photomechanical parameters (applied strain magnitude, irradiation time and intensity, and photoabsorber concentration) and the behavior of the network evolution rule on the material response.

© 2009 Elsevier Ltd. All rights reserved.

\* Corresponding author.

E-mail address: [Martin.Dunn@colorado.edu](mailto:Martin.Dunn@colorado.edu) (M.L. Dunn).

## 1. Introduction

Environmentally activated polymers are an exciting class of materials that deform in response to activation by an environmental stimulus. Recently, much attention has been devoted to understand and characterize the coupled environmental-mechanical response in the context of the shape-memory effect, wherein a material stores a temporary shape until a specified change in the environment causes the material to return to a permanent shape. Temperature has been the most common and perhaps best understood environmental stimulus (see, e.g., Liu et al., 2006; Nguyen et al., 2008; Qi et al., 2008). However, chemical, optical, electrical, and magnetic fields have also recently been demonstrated (Buckley et al., 2006; Huang et al., 2005; Lendlein and Kelch, 2002; Monkman, 2000; Schmidt, 2006). One way these mechanisms work is to indirectly activate the thermal shape-memory effect, either by producing a temperature change that spans an appropriate transition temperature of the polymer or by changing the transition temperature relative to the environment. For example, Behl and Lendlein (2007) demonstrated a thermoplastic shape-memory polymer (SMP) with embedded iron(III)oxide core/silica shell nanoparticles that convert energy from a remotely applied alternating magnetic field into heat which subsequently changes the shape of the material.

Recently, light-activated polymers have been developed that exhibit large macroscopic deformation, as well as the shape-memory effect, when irradiated by light at specified wavelengths. The underlying mechanisms that drive light-activated polymer deformation, however, are quite different from those that drive thermally induced shape memory. Light as a stimulus is particularly intriguing because it allows actuation of polymeric materials and devices without physical contact and offers the potential to control the location where the stimulus is applied. Indeed various optical technologies can be used to generate light incident on a polymer with both spatial and temporal control of the intensity and wavelength. This permits a wide range of potential applications for these materials including sensors and actuators from the millimeter-scale to the nanometer-scale, remotely deployable structures in aerospace applications, remotely triggered drug delivery systems, non-invasive surgery and implant devices in biomedicine, and stress-free dental composite cures (Liu et al., 2004; Scott et al., 2006; Tobushi et al., 1996; Yakacki et al., 2007).

A number of different polymer systems are actuated by light and exhibit the shape-memory effect. Perhaps the most studied materials are liquid crystal elastomers (LCEs) that contain light-sensitive molecules (Finkelmann et al., 2001; Hogan et al., 2002; Cviklinski et al., 2002; Li et al., 2003; Warner and Terentjev, 2003). The molecular structure of these materials consists of stiff, ordered, rod-like photoisomerizable functionalities embedded in an elastomeric network that can be reversibly bent upon irradiation at particular wavelengths. Due to the coupling between the orientational order of the rods and the mechanical deformation of the network, controlled macroscopic deformation is obtainable. These materials are attractive because the photomechanical coupling is reversible, although light of different wavelengths is required for the forward and backward processes. They can exist as thin monodomain or polydomain films. Recently, another class of photomechanically coupled polymeric materials, including the materials developed by Lendlein et al. (2005), Jiang et al. (2006), and by Scott et al. (2005, 2006), have emerged with a photoactivation mechanism quite different from that of LCEs. In these materials, photoactivation is achieved through photochemically induced network adaptation/rearrangement, which leads to changes of the mechanical states of the material. Advantages of these new materials include that they can be fabricated in bulk quantities, can exist in both rubbery and glassy states, and can exhibit the shape-memory effect.

Lendlein et al. (2005), Jiang et al. (2006) developed an amorphous, covalently crosslinked polymer with photo-tunable molecular crosslinks (PMC). Here, pendant chromophores (photo-sensitive functional groups) are attached to the polymeric backbone. Upon irradiation at wavelengths longer than 260 nm, the chromophores dimerize, chemically bonding together and providing additional crosslinking. These crosslinks can be photocleaved by irradiation at wavelengths shorter than 260 nm (Lendlein et al., 2005). A schematic showing the chromophore molecules in their bonded and unbonded state is presented in Fig. 1. This mechanism was exploited to demonstrate photo-induced shape memory. Initially, a sample is deformed from its original shape and held during irradiation at  $\lambda > 260$  nm. During this process light propagates through the material reacting with the chromophores, dimerizing the chromophores, and introducing a secondary set of crosslinks,

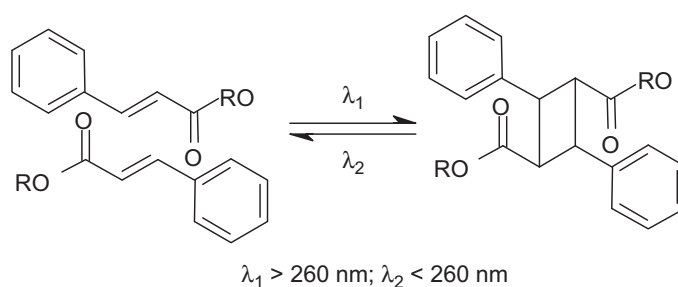


**Fig. 1.** Schematic of the photo-induced bonding and cleavage of chromophore functional groups in the PMC network. R indicates continuation of the polymer chain. Two chromophore molecules are shown in their unbonded (left) and bonded states (right). In the bonded state, each chromophore pair provides the polymer network an additional crosslink. Irradiation at wavelengths above (below) 260 nm drives the population of chromophores to bond (cleave) (Jiang et al., 2006).

or effectively a secondary network. From a mechanics perspective, the behavior of this second network differs from that of the original network because it references the deformed geometry as its stress-free configuration. After UV irradiation, the sample is released from its external constraints, but due to the formation of the secondary network, which has a different reference state than the original network, the sample deforms to an intermediate shape and remains in this geometry. Recovery to its original shape is achieved via a second irradiation at  $\lambda < 260$  nm, causing photocleavage of the chromophore dimers. During these processes, the material is maintained above its glass transition temperature ( $T_g$ ) to ensure sufficiently fast photochemical reaction rates relative to the laboratory time scale (minutes to hours).

Scott et al. (2005, 2006) recently developed a photomechanical polymer that is capable of photo-induced stress relaxation at particular wavelengths. This material is also an amorphous, covalently crosslinked, polymer network operated well above its  $T_g$ ; however, the molecular mechanism for photo-induced actuation is somewhat different. Irradiation of the material cleaves embedded photoinitiator molecules which chemically dissociate into free radical fragments. This process is shown in Fig. 2a. These free radicals then react via addition to and subsequent fragmentation of the polymer backbone. A schematic of the radical-induced rearrangement of the polymer backbone is shown in Fig. 2b. As this radical addition/fragmentation reaction with the polymer backbone is energetically reversible, individual addition/fragmentation events contribute little to changes in the polymer network. Indeed, radical-induced rearrangement does not alter the polymer chemistry or average crosslink density/modulus (Scott et al., 2006). However, many such events *permanently* alter the polymer network structure. The aggregate effect of many radical cleavage/reformation events restores the polymer network to its highest entropy configuration; any order in the network, such as partial chain alignment due to imposed mechanical deformations, is eliminated. Macroscopically, this process results in photo-induced stress relaxation. Radicals are conserved through the addition/fragmentation reaction and undergo many such backbone rearrangements prior to their inactivation by termination. When used in a shape-memory setting, the material is deformed from its original configuration and then irradiated while the deformation is maintained. The irradiation is intentionally non-uniform through the sample thickness so that the photo-induced stress relaxation is correspondingly non-uniform. When the external load is then released, the material deforms to an intermediate shape with a new residual stress distribution dictated by equilibrium. A second irradiation further relaxes the residual stresses and returns the material to its original shape. Appropriately tailored non-uniform irradiation protocols produce multiple stable intermediate shapes. In essence, this material operates as a result of photo-induced network rearrangement (PNR). As compared to the PMC material described above, realization of the stored shape for the PNR material is more complex as it strongly depends both on the applied stress/strain used to deform the material as well as the non-uniform stress relaxation that occurs upon irradiation.

To fully realize application potential, it is necessary to develop a thorough understanding of the macroscopic photomechanical behavior of light-activated polymers as determined by the underlying photophysical and photochemical mechanisms. This understanding can then be incorporated into mechanism-based models of photomechanical behavior

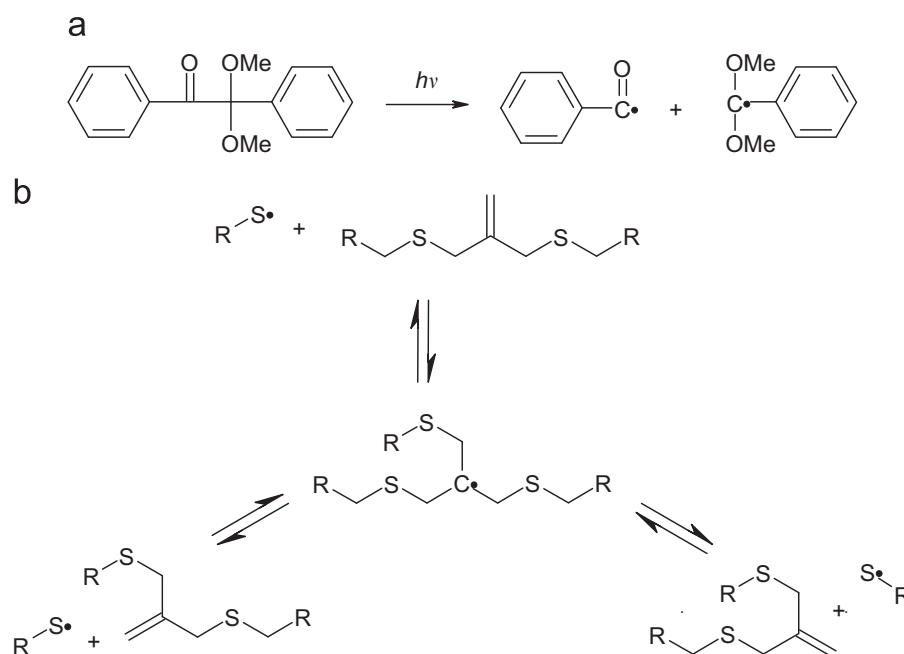


**Fig. 2.** (a) Schematic of the photochemical reaction of the Irgacure 651 initiator used in the PNR material. Two free radicals are developed in this process though the carbon-centered radical with two ether groups (on the right) may further degrade. Here, “Me” indicates a methyl group. (b) Schematic of the radical-mediated polymer backbone rearrangement in the PNR material. R indicates continuation of the polymer backbone. Addition of a sulfur-centered radical fragment to the carbon-carbon double bond yields an unstable carbon-centered radical intermediate. Spontaneous fragmentation of the unstable intermediate yields one of three possible network connectivities, conserving the carbon-carbon double bond and radical concentrations (Scott et al., 2006).

that are used in a design setting. This work constitutes a first step in this direction. We develop a model to simulate the photomechanical behavior of light-activated polymers (applicable to both the PNR and PMC materials) that can be applied to polymer systems with various operative molecular mechanisms. Our modeling approach incorporates the effects of light propagation through the solid, the photochemistry responsible for network evolution, the resultant chemical–mechanical coupling, and finally the large-deformation mechanical response. Our model is developed in a full three-dimensional finite-deformation framework and is implemented in a finite element setting. We use a suite of photomechanical experiments using PNR materials to guide our modeling efforts, as well as to determine relevant physical parameters for the model. We then simulate the photo-induced bending behavior of light-activated polymer samples and compare the results to companion experiments. Finally, we investigate the effects of important photomechanical parameters on material response, with a view toward the development of novel actuator materials and structures.

## 2. Materials and experiments

We designed and carried out a suite of experiments with the recently developed photo-induced network rearrangement materials described in the previous section. Complete details regarding the material synthesis, sample preparation, and photomechanical experiments have been described elsewhere (Scott et al., 2005, 2006; Cook et al., 2008), and so here we only briefly describe the relevant details.

Resin consisting of 75 wt% of a stoichiometric ratio of pentaerythritol tetra(3-mercaptopropionate) (PETMP) and 2-methylene-propane-1,3-di(thioethylvinylether) (MDTVE), and 25 wt% 2-methyl-7-methylene-1,5-dithiacyclooctane (MDTO), was formulated with two photoinitiators, 1.0 wt% Irgacure 819 and 2.0 wt% Irgacure 651. Irradiation of the uncured, formulated resin with visible light at  $40 \text{ mW cm}^{-2}$ , 400–500 nm, consumes Irgacure 819, generating radicals and initiating the polymerization. Irgacure 651 does not absorb visible light and thus is not consumed during the polymerization. Consequently, it is available for the generation of radicals in cured specimens upon ultraviolet irradiation (365 nm). A second set of samples was fabricated that additionally contained 0.5 wt% Tinuvin 328, an ultraviolet absorber, before polymerization. These samples were designed to strongly attenuate ultraviolet light, making it easier to develop well-controlled light intensity gradients through the sample upon irradiation. We refer to the latter samples as *optically thick* and the former as *optically thin* because of the way light is attenuated when propagating through them. While the addition of the photoabsorber strongly influences the propagation of light through the sample, it does not influence the mechanical properties. The  $T_g$ , determined as the peak in  $\tan \delta$  using dynamic mechanical analysis, is  $-22^\circ \text{C}$  and the modulus at room temperature is 9.5 MPa.

The basic testing protocol for all photomechanical experiments consists of subjecting flat strips (approximately 30 mm ( $L$ )  $\times$  8 mm ( $W$ )  $\times$  0.15 mm ( $T$ )) to uniaxial tension to a prescribed strain. For all samples, an MTS Insight 2 testing system was used with a 10 N full capacity load cell. While being held at this strain, the samples were irradiated with light, and the stress necessary to keep them fixed at the applied strain was measured during irradiation. The region of the surface that was irradiated, the intensity of light, and the irradiation time were all parameters that varied from test to test. The light was then turned off and the samples released from the grips. The samples then deformed and the equilibrium shapes were measured. Within this general protocol, we conducted two variations of tests, differing in the nature of the irradiation:

1. Uniform irradiation along one side of the strip with an optically thin sample so that the light intensity was also uniform through the thickness. These samples were strained in uniaxial tension at a strain rate of  $0.005 \text{ min}^{-1}$  to prescribed strains of 3.5%, 4.5%, 6%, and 7.5%. The samples were held at these strains for 60 s and then were irradiated at 365 nm and  $40 \text{ mW cm}^{-2}$  for 800 s while the constraint was maintained. The light irradiated each sample nearly uniformly, both in the plane of the sample and through its thickness. Stress relaxation was observed and measured during the irradiation process as shown schematically in Fig. 3a. The intent here is to characterize the uniform stress relaxation that occurs during irradiation and to determine the material parameters for the model described in the next section.
2. Patterned irradiation along both sides of an optically thick sample so that the light intensity varies both in the plane and through the thickness of the sample. The samples were photo-patterned with alternating 7 mm aluminum masks on either side. They were subjected to a tensile strain of 6% and then irradiated at 365 nm and  $10 \text{ mW cm}^{-2}$  for 180 s. The samples were then released from the mechanical grips, and they deformed into a wavy shape as shown schematically in Fig. 3b. The intent here is to induce non-uniform stress relaxation both in the plane and through the thickness that results in controllable, but more complex, deformation upon release of the mechanical constraints. These results will be used to demonstrate the photo-actuation capability of the material as well as the ability of our model to describe this process.

## 3. Modeling the photomechanics

To develop a general constitutive modeling framework for light-activated polymers, we consider the physical events in a typical photomechanical scenario common to both PMC and PNR systems. First the material is deformed from its original shape to an intermediate shape and held in this configuration. It is then irradiated at a specified wavelength. As the light

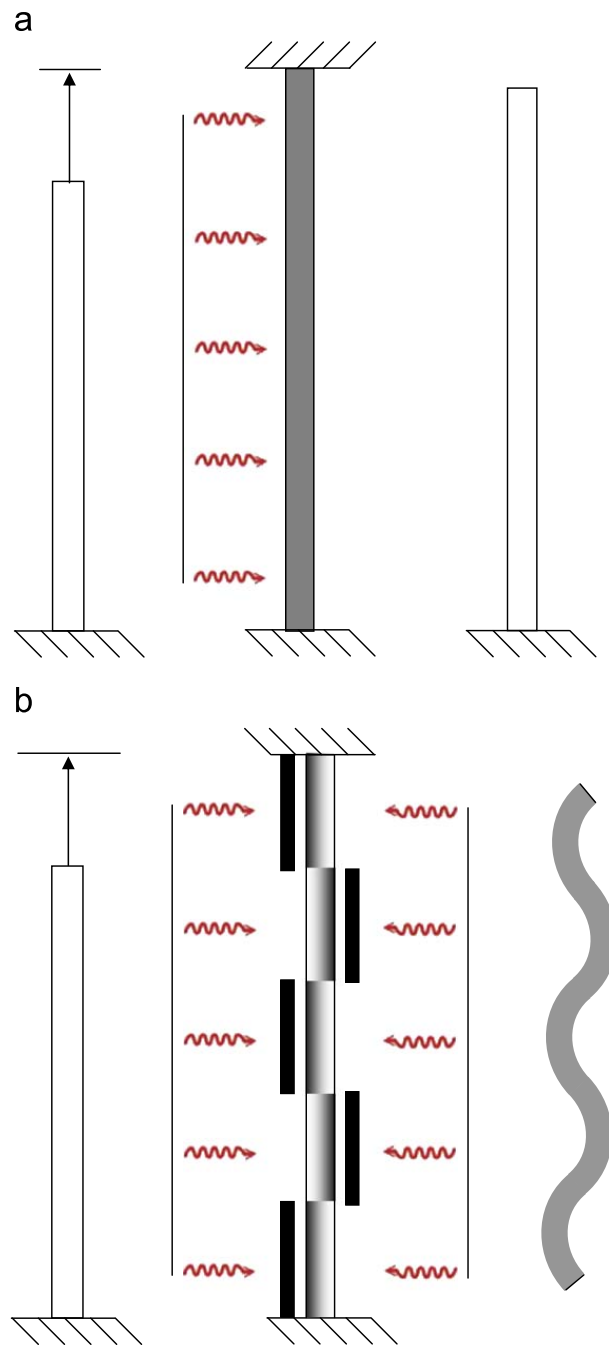


**Fig. 3.** (a) Schematic of the photomechanical testing protocol for photo-induced stress relaxation. First, a sample is stretched and held, then uniformly irradiated from one side. Upon release, the structure nearly maintains the deformed geometry. (b) Schematic of the test procedure to develop an oscillatory structure. The sample is stretched, held, and photo-masked. Irradiation from both sides results in patterned stress relief and an oscillatory structure upon release.

penetrates and propagates through the material, it initiates photochemical reactions. These reactions lead to changes in the polymer network structure and consequently alter the mechanical response of the material upon release of the mechanical constraints. The field equations for each of these steps and the general computational procedure will be discussed in the following sections.

Here, we assume the physical processes underlying the photochemistry and chemomechanical coupling are unaffected by the deformation state. For the PNR material, this assumption has been validated experimentally to moderate strains up to 7.5% as will be demonstrated and discussed in the results section. Moreover, in a mechanically analogous system of thermally induced structure alterations in elastomers, the state of deformation, up to order 100% strain, does not affect the rate of thermally induced changes to the polymer network (Tobolsky, 1960). We also make this assumption for the PMC material, but experimental verification is required in future work. At large deformation, optical properties of a polymer system may be affected by the state of deformation. In particular, inquiries have found that the refractive index of polymer

systems can be altered by large deformations (Treloar, 1958). As our work focuses on establishing a general modeling framework for the photomechanical behavior of light-activated polymers, we currently disregard such mechano-optical coupling; however, it can readily be added to our framework as needed.

Since the PNR and PMC materials share many common photochemical and chemomechanical features, we present models for both materials and make distinctions as necessary. Computational results will only be presented for the PNR material due to the limited experimental results for PMC materials in the literature.

### 3.1. Light propagation

The first step in the general framework is to model light propagation through the material with the principal objective of determining the intensity field throughout the sample. Initially, the material is assumed to be structurally and chemically homogenous without internal boundaries. Therefore, scattering events arise only from exterior boundaries, and thus are ignored in this work (Davis and Marshak, 2004). Moreover, we assume that the irradiation is monochromatic as used in the companion experiments and the light propagation in both the PNR and PMC materials is adequately described by the same physical equations.

Light propagation through a chemically homogenous medium without internal sources or scattering is described by the Beer–Lambert law, which states that in a one-dimensional setting the absorbance of light varies linearly with both the sample length and the concentration of light absorber. Absorbance  $A$  is defined as

$$A = -\ln\left(\frac{I}{I_0}\right), \quad (1)$$

where  $I_0$  is the intensity of incident light and  $I$  is the light intensity exiting the medium. The Beer–Lambert law states that

$$A = \alpha l c, \quad (2)$$

where  $l$  is the length of the light path,  $c$  is the concentration of light absorbing species, and  $\alpha$  is the molar absorptivity. Combining Eqs. (1) and (2), and defining  $\sigma = \alpha c$  yields:

$$\ln\left(\frac{I}{I_0}\right) = -\sigma l. \quad (3)$$

The equivalent differential form of Eq. (3) is

$$\frac{dI}{dx} = -\sigma I. \quad (4)$$

The three-dimensional version of the Beer–Lambert Law, known as the radiative-transfer equation (Davis and Marshak, 2004), is the extension of Eq. (4):

$$\boldsymbol{\Omega}(\mathbf{y}, t) \cdot \nabla I(\mathbf{y}, \boldsymbol{\Omega}, t) = -\sigma(\mathbf{y}, t)I(\mathbf{y}, \boldsymbol{\Omega}, t). \quad (5)$$

Here,  $\boldsymbol{\Omega}$  and  $\sigma$  are the direction of the light and extinction fields, respectively, which depend on the intermediate position,  $\mathbf{y}$ , and time,  $t$ . The term intermediate position describes the position of the body during irradiation. Because the body is initially deformed and held prior to irradiation, this position is different from the reference position,  $\mathbf{x}$ , of the body. Kinematic distinctions between different configurations will be clarified and discussed in Section 3.3. However, it is important to note that, in general, light propagation and photochemistry will not be solved in the material's initial configuration. The direction field describes the direction of propagation of the intensity field, and is often uniform in space and time. However, through photopatterning or application of multiple beams, the direction field can be strongly spatially dependent. The extinction field,  $\sigma(\mathbf{y}, t)$ , characterizes the spatial depletion rate of the intensity field and will be directly connected to the photochemistry in the following section. Eq. (5) models light propagation through both the PMC and PNR materials; however, their respective extinction fields are different as will be discussed.

### 3.2. Photochemistry

For the PNR material, light propagation through the material induces a sequence of photochemical events. Photons react with embedded photoinitiator molecules which chemically disassociate into free radical molecules. These radicals reactively diffuse along the polymer backbone cleaving and reforming it; this mechanism underpins the network alternation and photomechanically induced stress relaxation.

The production of free radicals during the photoinitiation process is modeled as

$$\frac{\partial C_R(\mathbf{y}, t)}{\partial t} = m \frac{[\alpha_i \phi_i C_I(\mathbf{y}, t) I(\mathbf{y}, t)]}{N_A h \nu} + D_R \nabla^2 C_R(\mathbf{y}, t) - k_{Term}(C_R(\mathbf{y}, t))^n, \quad (6)$$

where  $C_R$  and  $C_I$  are the concentration fields of free radicals and initiators, respectively;  $N_A$ ,  $h$ , and  $\nu$  are Avogadro's number, Planck's constant, and the monochromatic frequency of light chosen specifically for cleavage of the photoinitiator. The first term on the right-hand side of Eq. (6) considers the generation of free radicals due to photon-initiator reactions. For each

initiator photochemical disassociation,  $m$  free radical molecules are produced, where  $m$  is an integer. In the system considered here,  $m$  is two (Goodner and Bowman, 2002). Note that not all photons absorbed by initiator molecules lead to photo-cleavage events; instead, a quantum efficiency,  $\phi_i$ , is associated with this process and is here assumed to be one-half (Faria and Steenken, 1997). The constant,  $\alpha_i$ , characterizes the molar absorptivity of the initiator concentration field. Since diffusion may occur if the radicals are spatially non-uniformly distributed, a Fickian diffusion term (the second term on the right-hand side of Eq. (6)) is included here with an isotropic diffusivity,  $D_R$ , for the radical species. The radical field equation also includes a termination term to account for the inactivation of radical species. Termination occurs when two radicals encounter, recombine and annihilate each other. Two constants characterize the rate of termination,  $k_{term}$  and  $n$ . The first constant is difficult to determine experimentally and is estimated in our analysis. The second constant,  $n$  or the termination exponent, defines how many radical molecules are needed per termination event.  $n$  can be estimated experimentally and for the PNR materials, is found to be unity (Cook et al., 2008; Scott et al., 2006).

The photo-cleavage process consumes photo initiators in order to produce free radicals. The evolution of photoinitiator concentration is described by

$$\frac{\partial C_I(\mathbf{y}, t)}{\partial t} = -\frac{[\alpha_i \phi_i C_I(\mathbf{y}, t) I(\mathbf{y}, t)]}{N_A h \nu} + D_I \nabla^2 C_I(\mathbf{y}, t). \quad (7)$$

Note that the first term on the right-hand side of Eq. (7) is different from the first term on the right-hand side of Eq. (6) by a factor of  $-m$ , reflecting the photoinitiator consumption concomitant with the production of  $m$  free radicals. Eq. (7) is an example of a first-order photochemical reaction model as it indicates that the time rate of change of the initiator concentration field is proportional to the product of the intensity field with itself. This is a standard modeling approach in the literature (Oadian, 2004; Terrones and Pearlstein, 2001). Similar to free radical diffusion, a Fickian diffusion term is also included characterized by the isotropic diffusivity,  $D_I$ , of photoinitiator. Diffusion is important in photopatterning scenarios where sharp gradients develop in the initiator concentration. Because the radical species propagate exclusively by reaction diffusion along the polymer backbone, one expects that the diffusivities of the initiator to be much larger than that of the radical species. However, through modeling the photoinitiator and radical concentration fields, variations in the radical diffusivity were found to contribute negligibly to the radical concentration profiles when compared with independent variations of the photoinitiator diffusivity. Therefore, for simplicity, the radical diffusivity is set equal to the initiator diffusivity throughout this analysis.

The photoinitiators, free radicals, and the polymer matrix, can all absorb photons and hence attenuate light as it propagates through the material. The attenuation of light is characterized by the extinction field:

$$\sigma(\mathbf{y}, t) = \alpha_I C_I(\mathbf{y}, t) + \alpha_R C_R(\mathbf{y}, t) + A_{matrix}, \quad (8)$$

where  $\alpha_I$  and  $\alpha_R$  are absorptivities of photoinitiators and free radicals, respectively.  $A_{matrix}$  is the absorption contribution of the matrix, which arises from the presence of embedded photoabsorbing molecules. In Eq. (8), complete photobleaching of the initiator is assumed, which indicates that the initiator fragments, other than radicals, generated during photoinitiation reactions do not absorb light. This assumption is made for simplicity but can easily be removed by adding another initiator-fragment extinction term in Eq. (8). As discussed before, two limiting light propagation scenarios exist as controlled by the extinction field: optically thin and optically thick. In optically thin systems, the intensity field is not significantly attenuated as light passes through the material. Consequently, the intensity and initiator fields exhibit little spatial variation throughout the thickness of the sample. These fields change temporally, but do not appreciably vary spatially. In the other extreme, an optically thick sample that is uniformly irradiated will exhibit strong spatial variation of the intensity and initiator concentration fields.

The photochemistry for the PMC material is slightly different from that for the PNR material. Here, light interacts with the chromophore functional groups causing them either to bond together (forward reaction) at wavelengths,  $\lambda > 260$  nm, or to cleave apart (backward reaction) at wavelengths,  $\lambda < 260$  nm. Since each bonded chromophore pair adds a crosslink to the network, the concentration of bonded chromophores is the main chemical quantity of interest for the PMC material. Following the previously discussed approach used to model photochemistry of the PNR system, the operative first-order photochemical reactions are described by

$$\frac{\partial C_{UB}(\mathbf{y}, t)}{\partial t} = -\left(\frac{\phi_{UB}(\nu) \epsilon_{UB}}{N_A h \nu}\right) C_{UB}^2(\mathbf{y}, t) I(\mathbf{y}, t) + 2\left(\frac{\phi_B(\nu) \alpha_B}{N_A h \nu}\right) C_B(\mathbf{y}, t) I(\mathbf{y}, t) \quad (9)$$

which states that the time rate of change of the unbonded chromophore concentration  $C_{UB}$  is proportional to the products of the unbonded ( $C_{UB}$ ) and bonded ( $C_B$ ) chromophore concentration fields and the light intensity field. The first term on the right-hand side gives the rate of photochemical reactions which combined unbonded chromophores into bonded chromophores. Here, it is assumed that the photochemical reaction is bi-molecular, requiring an exponent of 2, i.e. a photon in the presence of two unbonded chromophores is required to generate a bonded chromophore pair. The sign on the first term is negative because these photochemical reactions diminish the unbonded chromophore population. The second reaction is uni-molecular in the presence of light and hence has only a power of one. The sign on this term is positive with a prefactor of two since photo-cleaving a bonded chromophore results in two unbonded chromophores. The two functions  $\phi_{UB}(\nu)$  and  $\phi_B(\nu)$ , are the quantum efficiencies of the bonding and cleavage photochemical reactions and range between zero and one depending on the frequency. They are both frequency dependent and may be regarded as phenomenological

inputs determined experimentally. A simple form of these functions consistent with the physical scenario is

$$\phi_{UB}(v) = 1 \text{ and } \phi_B(v) = 0, \text{ if } v < v_C, \quad (10a)$$

for the case of bonding, and

$$\phi_{UB}(v) = 0 \text{ and } \phi_B(v) = 1, \text{ if } v < v_C, \quad (10b)$$

for the case of bond cleavage. In Eqs. (10a) and (10b),  $v_C$  represents the transition frequency below which the predominant photochemical reaction is to form chromophore bonds and above which to cleave them. In practice, the quantum efficiencies may vary significantly with frequency and may overlap each other over a range of frequencies. This latter possibility allows for a dynamic equilibrium of the forward and reverse chromophore photochemical reactions and may be important in modeling long time scale behavior of the photomechanical response as a function of frequency. Eqs. (9) and (10) predict hysteric behavior of the unbonded and bonded chromophore populations under irradiation periodic in frequency about  $v_C$ .

The total chromophore population, both unbonded and bonded, is a locally conserved quantity for the PMC material since the chromophores are functional groups bound to the polymer backbone. It is conceivable that a PMC material could be generated wherein the total chromophore population could vary across different regions of the sample, but the experiments and materials described are composed of a uniform distribution of chromophores (Lendlein et al., 2005). Therefore, the local conservation constraint on the total chromophore population takes the following form:

$$C_{UB}(\mathbf{y}, t = 0) = C_0, \quad (11a)$$

$$C_{UB}(\mathbf{y}, t) + 2C_B(\mathbf{y}, t) = C_0 \text{ for } t \geq 0. \quad (11b)$$

For the PMC material, following the same assumptions as for the PNR material, the extinction field can be defined as

$$\sigma(\mathbf{y}, t) = \alpha_{UB}C_{UB} + \alpha_B C_B + A_{matrix}, \quad (12)$$

where  $\alpha_{UB}$  and  $\alpha_B$  are the absorptivities of unbonded chromophores and bonded chromophores, respectively, and  $A_{matrix}$  is the absorption contribution of the polymer matrix.

### 3.3. Network structure alteration and evolution

To model the chemomechanical coupling, which provides the connection between the photochemistry and solid mechanics, the effects of the underlying molecular mechanisms must be connected to changes in the material at the macroscopic level. The PMC and PNR materials share a common characteristic that provides generality to the model; each photochemical event leads to structural changes in the polymer network. Consequently, the chemomechanical coupling is modeled through the parallel decomposition of the crosslinked network into multiple networks that *locally* account for the photo-history and associated changes of the polymer structure. Here, we use the concept of “multiple networks” to unify the structural changes in both the PNR and the PMC materials. In the PNR material, a portion of the polymer network reforms through the radical-mediated cleavage/reformation process; in the PMC material, bonded chromophores form additional crosslinking sites that effectively act as a new crosslinked network. The volume fractions of these photochemically altered networks are taken as internal state variables at material points to bridge the underlying molecular-scale photochemical mechanisms with the macroscopic material response. Furthermore, each network is distinguished by the kinematics associated with its stress-free configuration shown schematically in Fig. 4 and discussed below. Such a methodology has been successfully used by Tobolsky (1960), Wineman and Min (2003) and Wineman and Shaw (2004) to model thermally induced structural alterations in elastomers. The constitutive behavior of each of the individual network fractions is presented in Section 3.4.

For PNR materials, aggregate radical cleavage and reformation events result in a portion of the crosslinked network reforming in the deformed (intermediate) configuration,  $\mathbf{y}$ . This *reformed network* is stress-free in configuration  $\mathbf{y}$  (in which it was reformed). The remaining portion of the network, the *original network*, continues to reference the initial configuration,  $\mathbf{x}$ , as its stress-free state during subsequent deformation. We describe the local time evolution of the volume fractions of the original and reformed networks as

$$\frac{df_{original}}{dt} = H(C_R, f_{original}) = -k_1 C_R f_{original}^p, \quad (13a)$$

$$f_{original} + f_{reformed} = 1, \quad (13b)$$

$$f_{original}(t = 0) = 1, \quad f_{reformed}(t = 0) = 0. \quad (13c)$$

Here,  $f_{original}$  is the volume fraction of the original network. We assume the time rate of change of  $f_{original}$  is a function of the radical concentration and  $f_{original}$ . We explicitly assume a direct proportionality between the rate of change of the original network volume fraction and the radical concentration field through  $k_1$ . In addition, we assume that the rate of change is also dependent on the current volume fraction of the original network through the power of  $p$  to introduce photo-history effects as is observed in the experimental results as described in Section 4. Moreover, we assert that the total

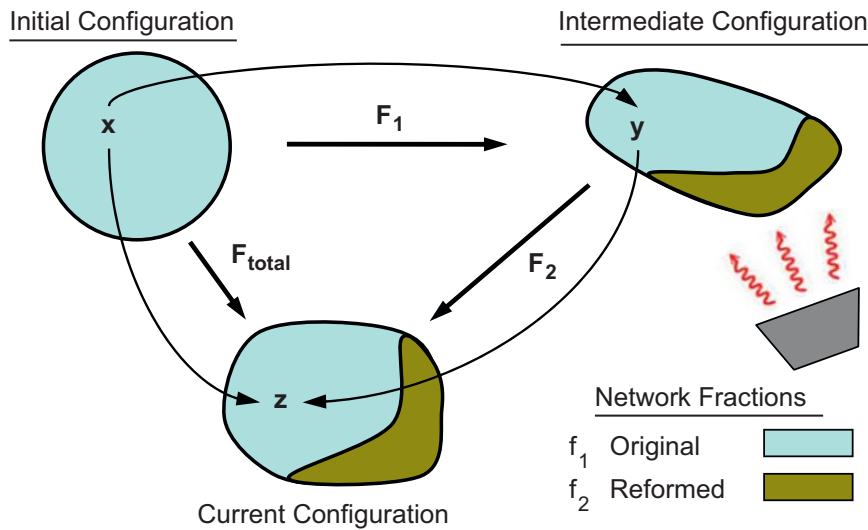


**Fig. 4.** Kinematics of the initial, intermediate, and current configurations. In the experimental protocols described, the sample, originally at  $x$ , is deformed to and held at an intermediate configuration,  $y$ . In this intermediate configuration, it is irradiated. After mechanical constraints are released, the sample deforms to the current configuration,  $z$ .

crosslink density is locally conserved by Eq. (13b) and that initially, the entire network is composed of the original network (Eq. (13c)). This first assertion is reasonable considering that the polymer chemistry and crosslink density are not affected by radical cleavage and reformation of the backbone as seen in Fig. 2b.

For the PMC material, chromophores provide additional photo-tunable crosslinks that are assumed here to act in parallel with the permanent set of crosslinks, which is unaffected by photomechanical treatments. As a result, we describe the evolution of the new crosslink density by

$$f_{new}(\mathbf{y}, t) = k_2 C_B(\mathbf{y}, t), \quad (14a)$$

$$f_{new}(t = 0) = 0. \quad (14b)$$

Here,  $f_{new}$  is the crosslink density associated with the chromophore–chromophore bonds;  $C_B$  is the concentration of bound chromophore pairs;  $k_2$  is a coefficient that relates the chromophore crosslink density to that of the permanent set of crosslinks. Note that  $f_{new}$ , as with  $C_B$ , is greater than or equal to zero for all time.

### 3.4. Constitutive behavior of the individual network fractions

Since both the PNR and the PMC materials are amorphous, chemically crosslinked polymers and function at temperatures above their respective glassy transition temperatures, it is reasonable to model them as incompressible, hyperelastic materials. For the PMC material, although the newly formed network may exhibit different mechanical behavior when compared to the permanent network, for the sake of simplicity, we assume that mechanical behavior of the two networks are described by the same constitutive model. For the PNR system, experiments have shown that there is an insignificant difference in mechanical behavior between the original and reformed networks; this result has been demonstrated via experiments on optically thin samples before and after uniform exposure to light (Scott et al., 2005). We, therefore, model the behavior of both the original and reformed networks with the same constitutive model. However, the mechanical behaviors of the networks are distinguished by the kinematics associated with their respective stress-free configurations as shown in Fig. 4.

For both the PMC and PNR materials, the photochemically altered network is assumed to be stress free in the configuration in which it is formed. The original network always references the initial configuration for its stress-free state. While the residual stresses generated during polymerization may be present in the initial state of the material, they are ignored in this analysis since they are small compared to subsequent applied stresses. In contrast to the original network, the photochemically altered network references an intermediate configuration dependent upon the photo-history. In the typical scenario shown in Fig. 4, the position of a material point,  $x$ , in the initial configuration, is tracked to its positions  $y$  and  $z$  in the intermediate and current configurations, respectively. The body is deformed from its initial configuration through the motion characterized by the deformation gradient and the left Cauchy–Green tensor,

$$\mathbf{F}_1 = \frac{\partial \mathbf{y}}{\partial \mathbf{x}}, \quad \mathbf{B}_1 = \mathbf{F}_1 \mathbf{F}_1^T. \quad (15)$$

This deformation is held while the body is irradiated; as a result of the photochemical interaction, a portion of the crosslinked network,  $f_2$  ( $f_2 = f_{reformed}$  for PNR, and  $f_2 = f_{new}$  for PMC), has either been created/destroyed or reformed for the PMC and PNR materials, respectively. When the light is switched off and the mechanical constraints are released, the body deforms again from the intermediate to the current configuration as described by the deformation gradient

$$\mathbf{F}_2 = \frac{\partial \mathbf{z}}{\partial \mathbf{y}}, \quad \mathbf{B}_2 = \mathbf{F}_2 \mathbf{F}_2^T. \quad (16)$$

In accordance with the general theory of non-linear hyperelasticity, the Cauchy stress in a given network is given by (Holzapfel, 2000)

$$\mathbf{T}_i = -p\mathbf{I} + 2 \left( \frac{\partial W_i}{\partial I_1^{(i)}} \mathbf{B}_i - \frac{\partial W_i}{\partial I_2^{(i)}} \mathbf{B}_i^{-1} \right), \quad i = 1, 2. \quad (17)$$

Here,  $W_{(i)}$  is the strain energy density function associated with  $i$ th network, and  $I_1^{(i)}$  and  $I_2^{(i)}$  are the first and the second invariants of  $\mathbf{B}_i$ . The pressure,  $p$ , accounts for the isochoric constraint on the deformation in purely incompressible materials (Holzapfel, 2000). Due to the parallel nature of the network decomposition, the total stress at a material point is the sum of the stresses in each network, i.e.

$$\mathbf{T}_{total} = f_{original} \mathbf{T}_1 + f_2 \mathbf{T}_2. \quad (18)$$

Although different energy functions exist for modeling hyperelasticity, we use the Arruda–Boyce eight-chain constitutive model to represent the mechanical behavior of all networks (Arruda and Boyce, 1993). This model uses Langevin chain statistics to properly account for the large stretch behavior of individual, freely jointed macromolecules assembled within an eight-chain network unit cell. This approach is appropriate for describing the behavior of entropically driven flexible polymer networks. An advantage of the Arruda–Boyce model is its relative simplicity; it contains only two material parameters that can be fit straightforwardly to experimental data. With the Arruda–Boyce model, the Cauchy stress for the  $i$ th network is given by

$$\mathbf{T}_i = \frac{\mu_r}{3} \frac{\sqrt{N}}{\lambda_{chain}^{(i)}} \mathcal{L}^{-1} \left[ \frac{\lambda_{chain}^{(i)}}{N} \right] \mathbf{B}_i - p\mathbf{I} \text{ with } \mathcal{L}^{-1}[\beta] = \coth[\beta] - \frac{1}{\beta}, \quad (19)$$

where  $\mu_r$  is the initial shear modulus, and  $N$  is the number of Kuhn lengths between crosslinks and therefore sets the locking stretch of the chain. The stretch of each chain in the network relates to the first invariant of  $\mathbf{B}_i$  through  $\lambda_{chain}^{(i)} = \sqrt{I_1^{(i)}/3}$ .

### 3.5. Thermal effects

For the specific PNR system modeled, thermal effects are insignificant and are neglected. In prior work the temperature change of similar, optically thick samples was measured to be approximately 5 °C throughout the entire photomechanical experiment (Scott et al., 2005). The samples used in those experiments were more than one millimeter in thickness, an order of magnitude larger than the samples used in the experiments presented here, and of similar widths. Therefore, we take the 5 °C measurement as an upper bound on the temperature change possible in the systems modeled here, and thus we neglect thermal effects. However, thermal effects can be important in PNR and PMC systems under a variety of conditions, including: strong absorption (optically thick); large intensities; insulating boundary conditions; highly exothermic photochemistry, etc. Significant temperature variation throughout the material could affect mechanical as well as photochemical properties. When thermal effects are important, the heat transfer problem can be readily implemented and coupled to the light propagation, photochemistry, and solid mechanics. The light propagation and photochemical field equations give the rates of matrix and radical absorption and photoinitiation which locally contribute to the rate of heat generation and can therefore be modeled as heat sources. The effects of radical-mediated structural rearrangement, and hence, stress relief in the network also influences the local rate of heat generation. With the local rate of heat generation available, a thermal boundary value problem can be solved subject to appropriate boundary and initial conditions.

### 3.6. Model implementation

All field equations are solved with second-order finite elements. The equations in the general framework are solved incrementally in time with the following sequence of steps per increment: the photochemical field equations are implemented in COMSOL MULTIPHYSICS, a flexible finite element platform, and solved using the sample geometry from the end of the previous time increment as the domain. The radical concentration field, stored at the nodes, is then passed to ABAQUS, another finite element software package, which solves for the chemomechanical coupling and the mechanical response via a user material subroutine. The current geometry (mesh) is exported from ABAQUS to COMSOL, and the cycle repeats with the next time increment. This sequential implementation can be viewed as a Forward Euler approach in coupling the photochemistry to the chemomechanical response. If large deformations are present during irradiation, many time increments will be required. However, if the sample is held during irradiation, as is the case in the photomechanical

scenarios presented in this work, the same intermediate geometry, with material point position  $\mathbf{y}$  in Fig. 4, can be used as the domain to model the photochemistry. Continuous deformation during irradiation can also be modeled incrementally by this approach which is important in cases where irradiation occurs while the sample is free of mechanical constraints.

#### 4. Results

In this section, we present simulation results, and compare them to measurements where possible, for various aspects of the photomechanical response of PNR materials. Our approach is to first present the behavior of the photophysical and photochemical fields. Then, we use the measured photomechanical stress relaxation data to determine parameters in the proposed network evolution laws. With these parameters known, we then predict the photomechanical behavior of both optically thin and thick samples and compare these predictions to measurements where possible. Finally, we study the influence of various macroscopic photomechanical parameters on material response as well as explore the behavior of the parameters that describe the underlying polymer network evolution. Due to limited experimental results on the PMC material, simulation results for the PMC material will not be presented.

In our experiments irradiation occurs nearly uniformly and normal to the exposed region. In our companion simulations, therefore, we assume that light propagates along a single direction normal to the sample surface and is otherwise uniform along any direction normal to the path of propagation. Both optically thin and optically thick photochemical systems are modeled to describe the systems with and without a photoabsorber. Photochemical constants used for these two scenarios, which are our experimental conditions, are summarized in Table 1; reference sources for the constants are included in the table caption. We note that the radical concentration field is of order  $10^{-9}$ – $10^{-7}$  mol L $^{-1}$  (Odian, 2004). Consequently, the radical termination constant,  $k_{term}$ , a difficult constant to measure experimentally, is chosen to set the order of magnitude of the radical field appropriately to  $10^{-8}$  mol L $^{-1}$ . At such a low concentration relative to the photoinitiator, the radical species does not significantly contribute to the extinction field, and therefore, for simplicity, the molar absorptivity of the radical species is assumed to be zero.

In Figs. 5a–c we show simulation results for the intensity (Fig. 5a), photoinitiator (Fig. 5b), and radical concentration fields (Fig. 5c) for a uniformly irradiated optically thin sample with no diffusion in which only the initiator absorbs light. For Figs. 5a and b, companion results from an available closed-form solution (Terrones and Pearlstein, 2001) are compared to the finite element results. Both the intensity and photoinitiator concentration fields are in excellent agreement with the analytical solutions, validating our numerical implementation. The intensity field initially shows some variation across the sample thickness, approximately 10% after 10 s of irradiation. At longer irradiation times, this variation disappears. This behavior is expected for an optically thin system because initially the photoinitiator absorbs and therefore attenuates the intensity field. Later, most photoinitiator molecules have already photochemically reacted and dissociated into radicals, and as the concentration of photoinitiators diminishes so does its associated contribution to the extinction field. Consequently, there is little attenuation of the intensity field at long irradiation times. The photoinitiator concentration field shows little variation at all times of interest across the sample thickness. Prior to irradiation, it is uniform, and once irradiation begins, the minor attenuation of the intensity field produces a small variation across the sample thickness that disappears at later times. The radical concentration field, with its production rate proportional to the photoinitiation rate, is also found to be nearly uniform throughout the sample thickness over the entire time range. These results are used in the simulation of the stress relaxation experiments for optically thin systems (without the photoabsorber) presented in the following sections.

Figs. 6a–c show the intensity (Fig. 6a), photoinitiator (Fig. 6b), and radical concentration fields (Fig. 6c) for a uniformly irradiated optically thick sample. Due to the presence of the photoabsorber, the intensity field is sharply attenuated through the sample, which results in non-uniform photoinitiation rates and, consequently, non-uniform photoinitiator and radical concentration profiles. After a long exposure period, shown at 300 s, the photoinitiator and radical concentration fields show less variation as the overall photoinitiation rate declines and diffusion smooths out concentration gradients.

**Table 1**

Photochemical constants used in the calculations of both optically thin and optically thick photomechanical modeling scenarios.

	Optically thin	Optically thick	Unit	Description
$\alpha_I$	118	118	L mol $^{-1}$ cm $^{-1}$	Photoinitiator molar absorptivity
$\alpha_R$	0	0	L mol $^{-1}$ cm $^{-1}$	Photo-radical molar absorptivity
$A_{Matrix}$	0	139	cm $^{-1}$	Photoabsorber extinction coefficient
$C_{I0}$	0.078	0.078	mol L $^{-1}$	Initial photoinitiator concentration field
$C_{R0}$	0	0	mol L $^{-1}$	Initial radical concentration field
$D_I$	1.0e–10	1.0e–10	m $^2$ s $^{-1}$	Initiator diffusivity
$D_R$	1.0e–10	1.0e–10	m $^2$ s $^{-1}$	Radical diffusivity
$I_0$	40	40 (10)	mW cm $^{-2}$	Incident intensity field
$k_{term}$	1.0e4	1.0e4	(L mol $^{-1}$ ) $^{n-1}$ s $^{-1}$	Radical termination constant
$m$	2.0	2.0	Dimensionless	Number of radicals developed per photoinitiation event
$n$	1.0	1.0	Dimensionless	Radical termination exponent
$\Phi_I$	0.5	0.5	Dimensionless	Quantum efficiency of photoinitiation
$Y$	8.213e14	8.213e14	Hz	Irradiation frequency

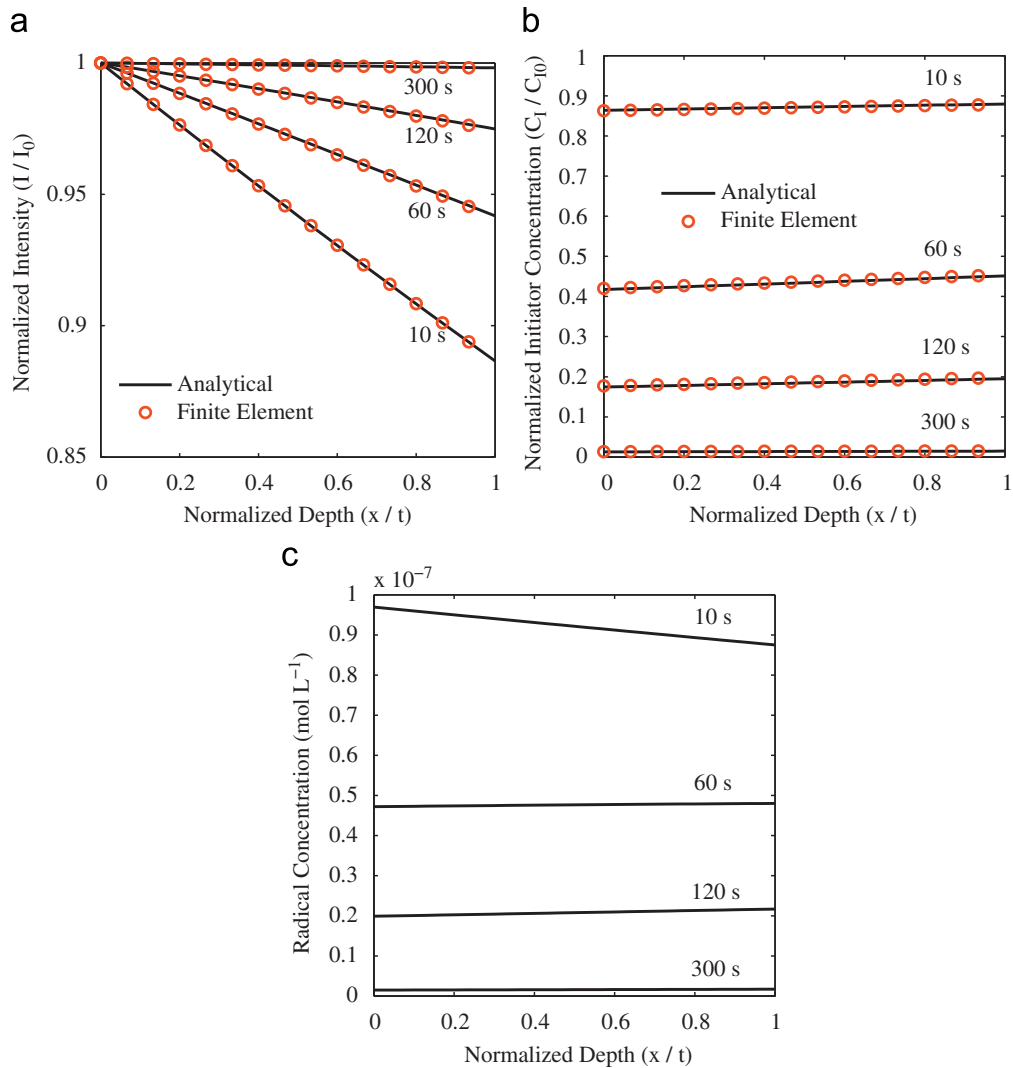


**Fig. 5.** Analytical and finite element calculations of (a) the light intensity, (b) the photoinitiator concentration, and (c) the radical concentration through a 1D, optically thin sample.

However, the intensity field is strongly attenuated at all times because of the continuing photoabsorber presence throughout the film. Additionally, it is important to note that the rate at which the photoinitiator field declines is markedly slower for the optically thick sample compared with the optically thin sample because the photoabsorber competes with the photoinitiator to absorb light.

A single optically thin photo-induced stress relaxation experiment at an applied normal strain of 6% was used to determine mechanical and network evolution parameters in the model. The measurements for both the loading and photo-induced stress relaxation were fit to photomechanical simulations (using the radical concentration field shown in Fig. 5c) to determine the mechanical constitutive parameters and the photomechanical parameters in the network evolution law. From these fits we determined the initial shear modulus and locking stretch parameters of the Arruda–Boyce model to be  $\mu_r = 3.3 \text{ MPa}$  and  $N \sim 10^4$ . Note that the large value of  $N$  implies that a neo-Hookean model might be sufficient for the material studied in this paper. The network structure evolution law parameters,  $k_1$  and  $p$ , were found to be  $300 \text{ m}^3 \text{ mol}^{-1} \text{ s}^{-1}$  and 1.0, respectively. These parameters were used with the photochemical and physical constants in Table 1 in all photomechanical simulations. The quality of the fit of the simulation data to the measurements is excellent as seen in Fig. 7. The model closely fits the initial, dramatic stress relaxation response as well as the transition region wherein the stress relaxation rate rapidly declines. Slight disagreement in the stress relaxation rate begins to develop between the model and measurement results after 10 min of exposure at which point the relative error is about 16%.

Fig. 7 in conjunction with Figs. 5a–c elucidates an important aspect of the PNR material. Specifically, the polymer network is fabricated with a finite concentration of residual initiator with which to generate free radicals. After a sufficient period of exposure, determined by experimental conditions such as the applied intensity, sample dimensions, and the initial residual initiator concentration, the initiator concentration is depleted, and free radicals can no longer be developed. As the radical population declines, so does the sample's capacity to exhibit photo-induced stress relaxation. For the

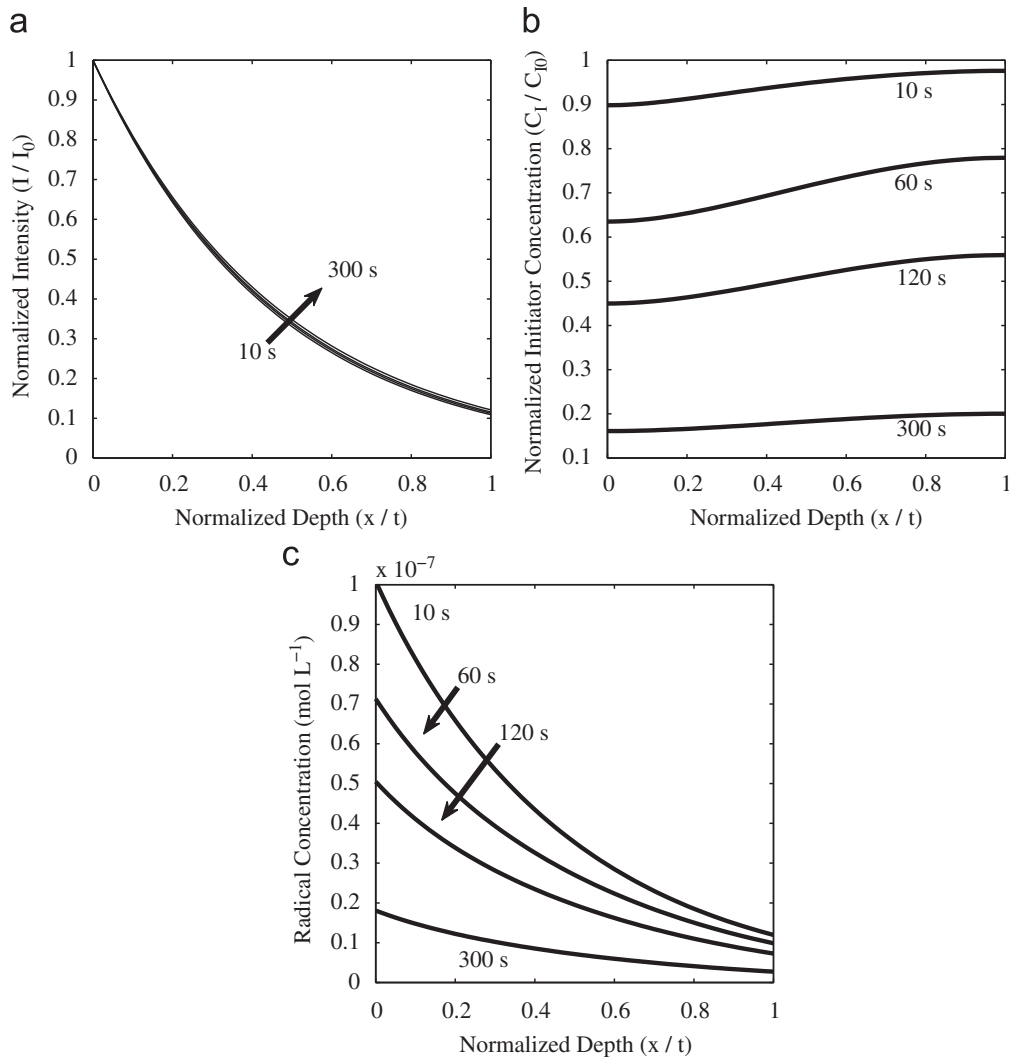


**Fig. 6.** Finite element calculations of (a) the light intensity, (b) the photoinitiator concentration, and (c) the radical concentration through a 1D, optically thick sample.

optically thin conditions explored in Figs. 5a–c, the initiator and radical concentrations decline by more than 95% after 300 s of exposure. A direct consequence is that the rate of stress relaxation is sharply diminished, a fact that is particularly evident in the semilog inset in Fig. 7.

Figs. 8a and b show measurements and predictions for photo-induced stress relaxation of optically thin samples at a range of prescribed strain values that differ from those used to determine the material parameters. The stress relaxation curves for each applied strain are normalized to their respective peak stresses in Fig. 8b. This normalization results in all three measurement curves collapsing onto a single master curve with minor variations existing only after long times. This suggests that the photo-induced stress relaxation of the PNR material does not depend on the state of mechanical deformation, at least up to nominal strains on the order of 10%. The experimental results support our assumption that the photochemistry is unaffected by the deformation state and hence the one-way coupling between the photochemistry and mechanical behavior built into the model framework. As a consequence of this assumption, the normalized simulation results exactly collapse onto a single curve which agrees well with the normalized experimental results.

Fig. 9 shows results for an optically thick sample, which contains a photoabsorber, that was stretched uniaxially and then subjected to non-uniform irradiation. As discussed previously, the sample was patterned on each side using a mask with a series of alternating 7 mm wide exposure/extinction windows. The pattern causes a non-uniform variation of the light intensity in the plane and since the sample is optically thick, the light attenuates strongly through the thickness as well. The concentration of the radical field thus varies non-uniformly through the solid, but in a predictable way. The variation through the thickness causes the sample to bend; the alternating patterns of exposure/extinction then provide a spatial variation of the bending, resulting in the wavy sample upon release of the mechanical constraint. The average curvature of the five segments is 0.180 and 0.167 mm<sup>-1</sup> for the experiment and simulation, respectively, which is a relative difference of 7.6%. The differences between experiment and simulation are slightly larger in the regions near the sample ends. However, the overall qualitative, as well as quantitative, behavior is clearly captured well by the model.

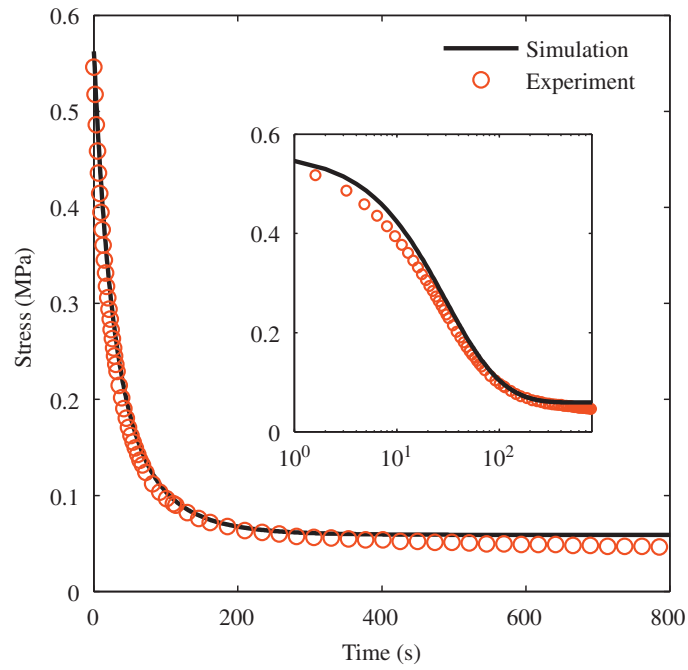


Fig. 7. Stress relaxation experimental and model fitting results for an optically thin sample. The inset plots the same results with a logarithmic scale for the time axis.

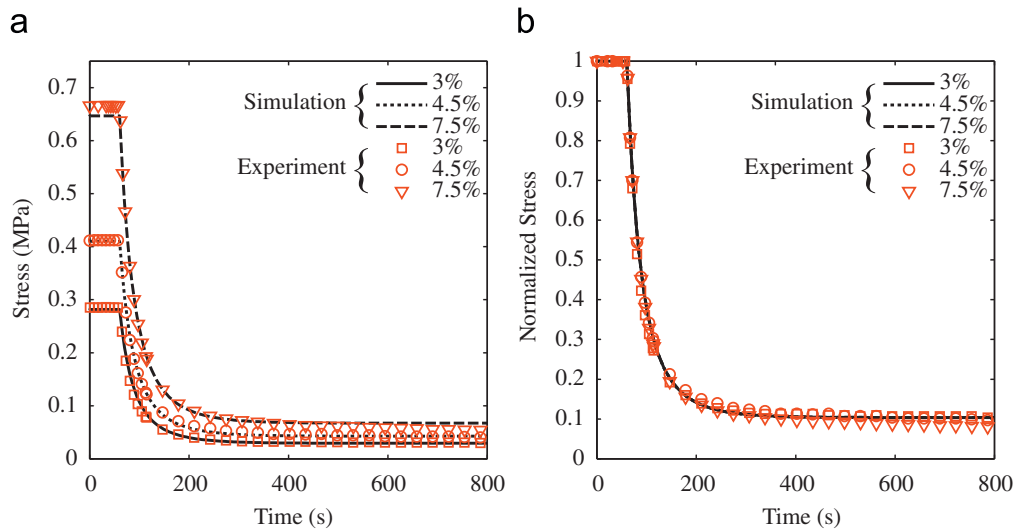


Fig. 8. (a) Stress relaxation experiments and model predictions for optically thin samples at different nominal strains. (b) Same plots as in (a) but with normalized stresses. Note that all curves nearly collapse to a single, master curve.

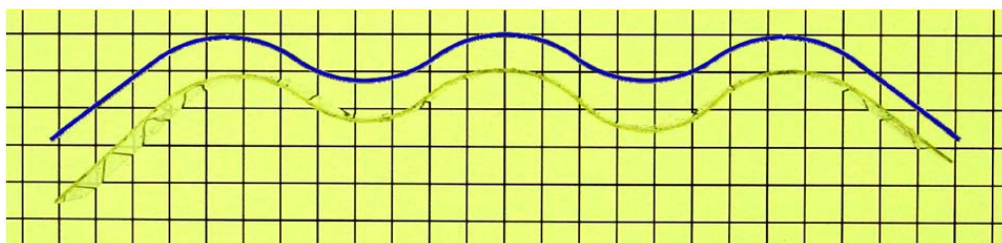
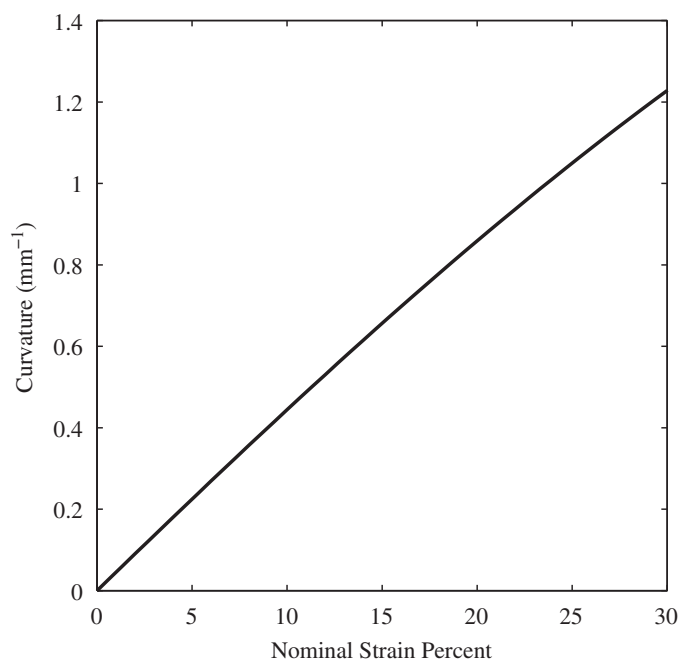


Fig. 9. Experimental (bottom) and simulation (top) results showing bending actuation via patterned irradiation of a photo-masked, optically thick sample.

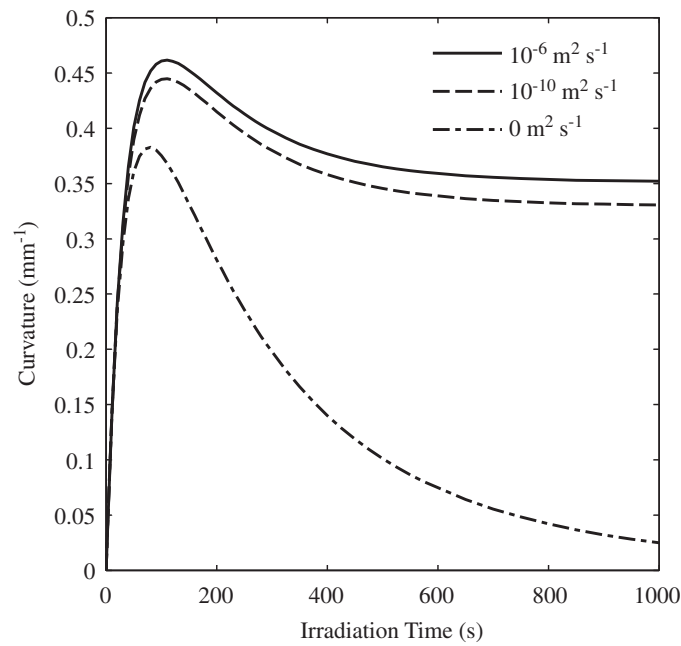


**Fig. 10.** Curvature of optically thick samples held at different strains during the illumination step. Control photochemical constants are 100 s of irradiation with  $40 \text{ mW cm}^{-2}$  intensity at 365 nm and a matrix absorption of  $139 \text{ cm}^{-1}$ .

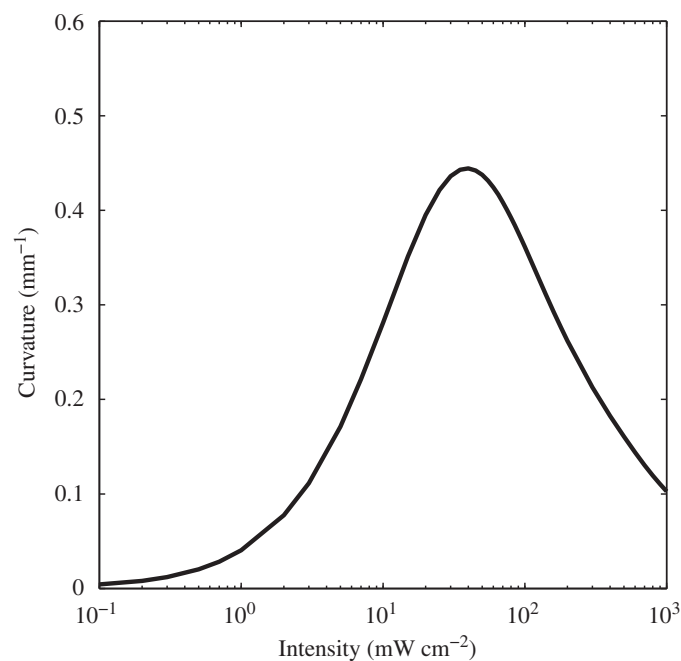
Actual applications will demand control over the photomechanical behavior of light actuated polymers. For the photo-induced bending actuation considered here, the curvature predominately characterizes the mechanical response, and so it is valuable to understand how various luminous, chemical, and mechanical parameters affect photomechanical bending behavior. To this end, we present results of a parametric study that explores the effects of the four most important macroscopic design parameters: applied strain, irradiation time, light intensity, and photoabsorber concentration. While the roles of the first three are likely clear, we note that the photoabsorber concentration provides a means to control the attenuation of the intensity field through the thickness, and thus the resulting stress relaxation and bending. The results of systematic variations of each of these four parameters are shown in Figs. 10–13. In the simulations used to develop these figures the material properties and photomechanical loading procedures previously described were employed with the following baseline parameters: nominal strain: 10%, irradiation parameters: 100 s,  $40 \text{ mW cm}^{-2}$  at 365 nm wavelength, and an absorption of  $139 \text{ cm}^{-1}$ .

Fig. 10 shows the curvature vs. applied strain, with all other photomechanical parameters held constant at the baseline values. The curvature increases monotonically with applied strain and exhibits only slight nonlinearity at larger strain values. This behavior is consistent with the uniaxial stress–strain behavior of the material as it is reasonably linear over strains well above 10%, and the photochemical response has been assumed and experimentally shown to be independent of the stress state. Thus, all simulation cases have the same normalized stress state throughout their respective bodies and differ only by the magnitude of the internal bending moment developed by the photo-induced stress relief. This internal bending moment scales directly with the peak stress, and the resultant curvature scales directly with the internal bending moment.

Fig. 11 shows the development of curvature with the time of irradiation for three cases intended to convey the effects of photoinitiator diffusion: (i) photoinitiator diffusion occurs as determined by the material properties in Table 1, (ii) the photoinitiator diffusivity is higher than its specification in Table 1, and (iii) the photoinitiator diffusivity is set to zero so that the effects of diffusion are not included in the simulation. For small exposure times light does not propagate significantly through the material and the radical fields change only close to the surface. As a result, little stress relaxation occurs, and so only a small stress gradient results through the sample thickness, and thus little curvature occurs. For small exposure times the three curves nearly match, suggesting that diffusion of the initiator and radicals does not play a role in the photomechanics. As the exposure time increases the behavior is more complex. In general, for long exposure times, more uniform stress relaxation occurs, resulting in a decreased stress gradient throughout the sample and a decreased curvature. In fact, if diffusion of the initiators and radicals did not occur during irradiation, the stress would uniformly relax over time and the curvature would tend to zero as shown in Fig. 12. When diffusion is considered, which is physically the appropriate situation here, the initiator concentration field is driven towards the irradiated side of the sample where it is continuously depleted. As a result, photoinitiation events and stress relaxation preferentially occur near the irradiated side of the material, and a net stress gradient is maintained, even at long exposure times. Between the short and long time exposure limiting cases the curvature develops a maximum. Without diffusion it is clear that a maximum must exist because the short- and long-term behavior results in no curvature. With diffusion, though, the existence and magnitude of this peak depend on the details of the initiator diffusion.



**Fig. 11.** Curvature of optically thick samples held at 10% strain and irradiated for different periods. Control photochemical constants are 10% nominal strain,  $40 \text{ mW cm}^{-2}$  intensity at 365 nm, and a matrix absorption of  $139 \text{ cm}^{-1}$  for three values of initiator diffusivity.



**Fig. 12.** Curvature of optically thick samples irradiated at different intensities. Control photochemical constants are 10% nominal strain, 100 s of irradiation at 365 nm, and a matrix absorption of  $139 \text{ cm}^{-1}$ .

In Fig. 12, we examine the effect of the light intensity during irradiation for 100 s. The curvature of the sample evolves with increasing intensity in the same manner as it does for increasing irradiation time, exhibiting a maximum at a finite intensity. The effect of the photoabsorber concentration on the sample curvature is shown in Fig. 13. Again, initially the curvature increases with increasing absorption, then reaches a maximum, and later decreases. Without the photoabsorber, for the composition and geometry of this material the sample is optically thin, and therefore, stress gradients and curvature are not produced. Hence, without the photoabsorber the curvature is zero. On the other extreme, if the absorption approaches an infinite value, no photochemical change is possible, and thus no stress is relieved. No curvature results; for intermediate absorption the sample assumes a maximum value of curvature.

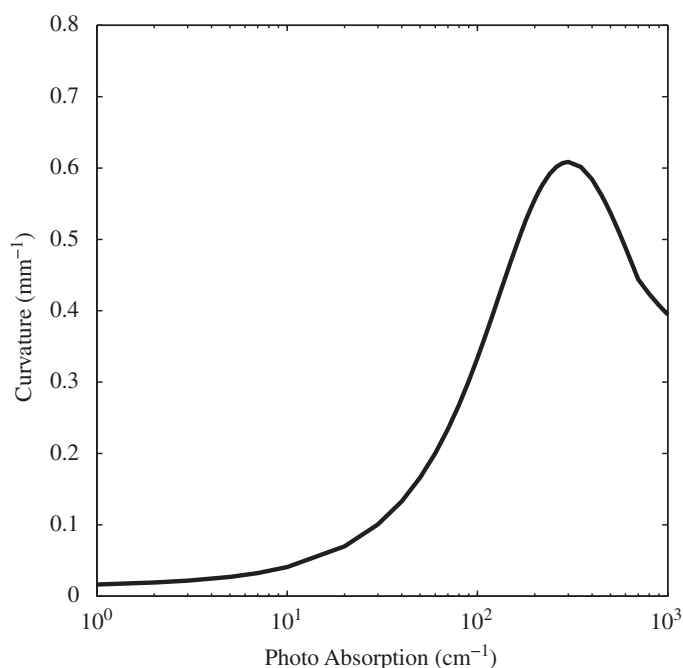


**Fig. 13.** Curvature of optically thick samples composed with different matrix absorption contributions to the extinction field. Control photochemical constants are 10% applied nominal strain and 100 s of irradiation with  $40 \text{ mW cm}^{-2}$  intensity at 365 nm.

The results in Figs. 10–13 indicate how to maximize the conversion of stored elastic strain energy from tension to bending. Indeed, the photomechanical process considered here for the PNR material may also be viewed from the standpoint of the development, conversion, and dissipation of stored elastic strain energy. The initial deformation of the material generates elastic strain energy at the expense of conformational entropy of the network. While the mechanical constraints are maintained, photochemical reactions induce network rearrangements that partially restore the conformational entropy of the network by diminishing the stored elastic strain energy ultimately as heat. Upon release of the mechanical constraints, the remaining stored elastic strain energy is released or redistributed to achieve mechanical equilibrium.

In Figs. 14 and 15, we explore the effects of the parameters  $k_1$  and  $p$  in the network evolution laws of Eqs. (13a)–(13c) on the photomechanical behavior. While  $k_1$  and  $p$ , were chosen to fit the PNR material behavior specifically, the evolution laws in Eqs. (13a)–(13c) can potentially be applied to represent different chemomechanical behavior of PNR materials and even to a broader class of materials that exhibit environmentally activated stress relaxation. To elucidate the characteristics of the network structural evolution laws, we performed photomechanical stress relaxation simulations with a radical concentration of  $10^{-8} \text{ mol L}^{-1}$  that is constant in time and uniform throughout the material. This concentration is of the same order of magnitude as the modeled concentrations in both the optically thin and optically thick systems.

As discussed in Section 3.3, the parameter  $k_1$  connects the stress relaxation rate to the radical concentration. Variations in  $k_1$  over four orders of magnitude are shown for a fixed value of  $p = 1$  in Fig. 14, which shows that increasing  $k_1$  amplifies the initial stress relaxation rate and sets the photomechanical time scale.

The effects of  $p$  are shown in Fig. 15 for a constant value of  $k_1$ . This parameter phenomenologically accounts for the radical history effects in the network, which may lead to premature radical termination events and the loss of efficiency of the stress relaxation mechanism. This behavior is clearly observed experimentally by the reduction in stress relaxation rates with time in Figs. 7 and 8. At small times, the stress relaxation does not depend strongly on  $p$ ; results for all four values of  $p$  collapse onto a single curve controlled by the value of  $k_1$ . For a fixed  $k_1$ , the parameter  $p$  determines the beginning of the transition region where the stress relaxation rate dramatically decreases. If  $p = 0$ , there are no radical history effects on the underlying mechanism, and the stress relaxation rate is constant until a zero stress state is observed. As  $p$  is increased, the onset of the transition region decreases, and consequently this limits the overall stress relaxation response.

## 5. Conclusions

We developed a modeling framework to describe the photomechanical behavior of light-activated polymers where photochemical reactions alter the polymer network structure, which results in deformation. Our framework is

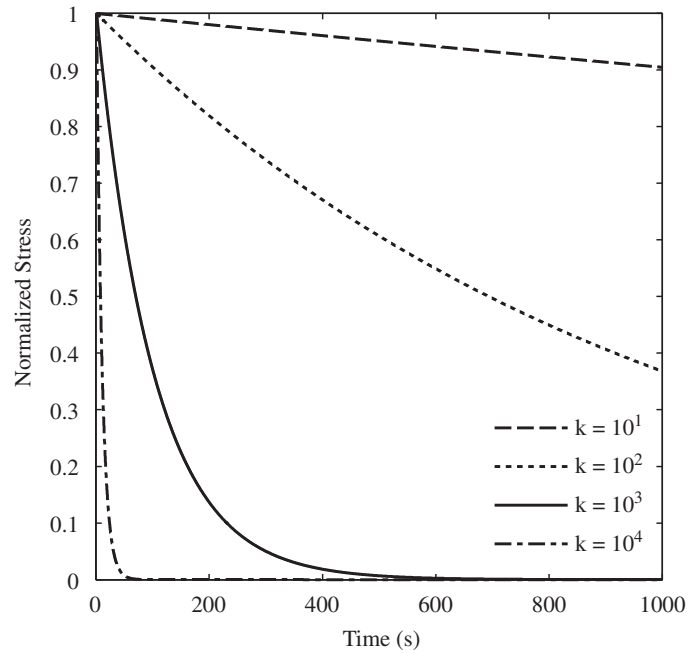


**Fig. 14.** The influence of the network structure evolution rule prefactor,  $k_1$ , on the stress relaxation behavior of an optically thin sample.

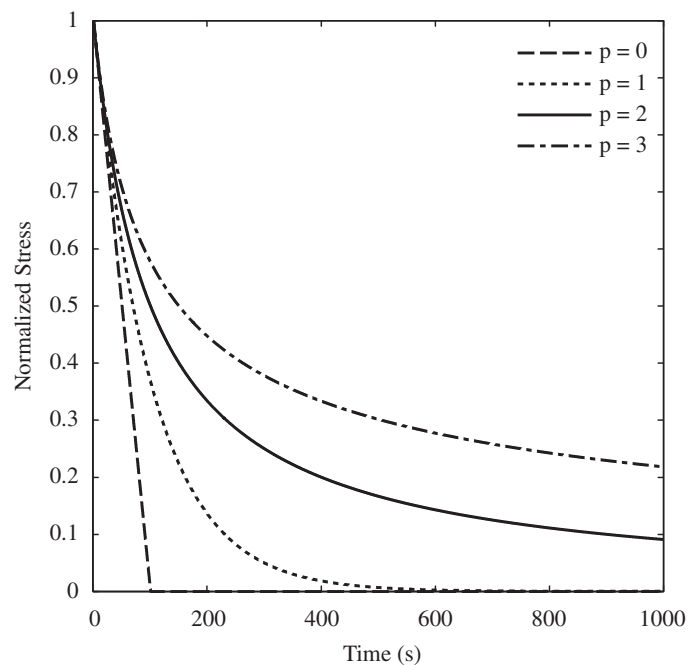


**Fig. 15.** The influence of the network structure evolution rule exponent,  $p$ , on the stress relaxation behavior of an optically thin sample.

implemented in a finite element setting and integrates four coupled phenomena that contribute to enable macroscopic photomechanical behavior: photophysics, photochemistry, chemomechanical coupling, and mechanical deformation. The chemomechanical coupling broadly consists of chemical alteration of the crosslinked network that results in subsequent deformation. We describe this through the decomposition of the crosslinked network into two components, an original network and a photochemically altered network; both evolve during photomechanical deformation. The proposed modeling framework is sufficiently general that it can be applied to light-activated polymer systems that operate with different mechanisms in each of the four areas. Model simulations compare nicely with experiments reported in literature. In addition, the developed model enables an investigation of the effects that the photomechanical and network evolution rule parameters have on the material response. Such a study promotes future development of novel actuators, structures, and advanced materials based on these light-activated polymer systems.

## Acknowledgments

We gratefully acknowledge the support of the Air Force Office of Scientific Research MURI (Grant F9550-06-1-0326) monitored by Dr. B.L. Lee (MLD), an NSF Career award (CMMI-0645219), a grant from the NSF-Sandia initiative (Sandia National Laboratories, 618780) (HJQ), a grant from the National Institutes of Health (DE-10959) (CNB, TFS) and an NSF Graduate Research Fellowship (ID 2007056220) (KNL).

## References

- Arruda, E.M., Boyce, M.C., 1993. A three-dimensional constitutive model for the large stretch behavior of rubber elastic materials. *Journal of the Mechanics and Physics of Solids* 41 (2), 389–412.
- Behl, M., Lendlein, A., 2007. Shape-memory polymers. *Materials Today* 10 (4), 20.
- Buckley, P.R., McKinley, G.H., Wilson, T.S., Small Iv, W., Bennett, W.J., Beringer, J.P., McElfresh, M.W., Maitland, D.J., 2006. Inductively heated shape memory polymer for the magnetic actuation of medical devices. *IEEE Transactions on Biomedical Engineering* 53 (10), 2075.
- Cook, W.D., Chausson, S., Fei, C., Le Pluart, L., Bowman, C.N., Scott, T.F., 2008. Photopolymerization kinetics, photothology and photoplasticity of thiol-ene-allylic sulfide networks. *Polymer International* 57 (3), 469.
- Cviklinski, J., Tajbakhsh, A.R., Terentjev, E.M., 2002. UV isomerisation in nematic elastomers as a route to photo-mechanical transducer. *European Physical Journal E* 9 (5), 427–434.
- Davis, A.B., Marshak, A., 2004. Photon propagation in heterogeneous optical media with spatial correlations: enhanced mean-free-paths and wider-than-exponential free-path distributions. *Journal of Quantitative Spectroscopy and Radiative Transfer* 84 (1), 3.
- Faria, J.L., Steenken, S., 1997. Photoionization of  $\alpha$ -alkoxybenzyl radicals to yield  $\alpha$ -alkoxybenzyl cations. *Photochemistry of  $\alpha$ , $\beta$ -dimethoxy- $\beta$ -phenylacetophenone in polar solvents at high light intensities. Journal of the Chemical Society, Perkin Transactions 2*, 1153–1159.
- Finkelmann, H., Kim, S.T., Munoz, A., Palffy-Muhoray, P., Taheri, B., 2001. Tunable mirrorless lasing in cholesteric liquid crystalline elastomers. *Advanced Materials* 13 (14), 1069–1072.
- Goodner, M.D., Bowman, C.N., 2002. Development of a comprehensive free radical photopolymerization model incorporating heat and mass transfer effects in thick films. *Chemical Engineering Science* 57 (2002), 887–900.
- Hogan, P.M., Tajbakhsh, A.R., Terentjev, E.M., 2002. UV manipulation of order and macroscopic shape in nematic elastomers. *Physical Review E* 65 (4).
- Holzappel, G.A., 2000. *Nonlinear Solid Mechanics: a Continuum Approach for Engineering*. Wiley, Chichester, England.
- Huang, W.M., Yang, B., An, L., Li, C., Chan, Y.S., 2005. Water-driven programmable polyurethane shape memory polymer: demonstration and mechanism. *Applied Physics Letters* 86 (11), 114105.
- Jiang, H., Kelch, S., Lendlein, A., 2006. Polymers move in response to light. *Advanced Materials* 18 (11), 1471.
- Lendlein, A., Hongyan, J., Junger, O., Langer, R., 2005. Light-induced shape-memory polymers. *Nature* 434 (7035), 879.
- Lendlein, A., Kelch, S., 2002. Shape-memory polymers. *Angewandte Chemie-International Edition* 41 (12), 2035.
- Li, M.H., Keller, P., Li, B., Wang, X.G., Brunet, M., 2003. Light-driven side-on nematic elastomer actuators. *Advanced Materials* 15 (7–8), 569–572.
- Liu, Y., Gall, K., Dunn, M.L., Greenberg, A.R., Diani, J., 2006. Thermomechanics of shape memory polymers: uniaxial experiments and constitutive modeling. *International Journal of Plasticity* 22 (2), 279.
- Liu, Y., Gall, K., Dunn, M.L., McCluskey, P., 2004. Thermomechanics of shape memory polymer nanocomposites. *Mechanics of Materials* 36 (10), 929.
- Monkman, G.J., 2000. Advances in shape memory polymer actuation. *Mechatronics* 10 (4–5), 489.
- Nguyen, T.D., Jerry Qi, H., Castro, F., Long, K.N., 2008. A thermoviscoelastic model for amorphous shape memory polymers: incorporating structural and stress relaxation. *Journal of the Mechanics and Physics of Solids* 56 (9), 2792.
- Odian, G., 2004. *Principles of Polymerization*. Wiley-Interscience, Staten Island, New York.
- Qi, H.J., Nguyen, T.D., Castro, F., Yakacki, C.M., Shandas, R., 2008. Finite deformation thermo-mechanical behavior of thermally induced shape memory polymers. *Journal of Mechanics and Physics of Solids* 56, 1730–1751.
- Schmidt, A.M., 2006. Electromagnetic activation of shape memory polymer networks containing magnetic nanoparticles. *Macromolecular Rapid Communications* 27 (14), 1168.
- Scott, T.F., Draughon, R.B., Bowman, C.N., 2006. Actuation in crosslinked polymers via photoinduced stress relaxation. *Advanced Materials* 18 (16), 2128.
- Scott, T.F., Schneider, A.D., Cook, W.D., Bowman, C.N., 2005. Photoinduced plasticity in crosslinked polymers. *Science* 308 (5728), 1615.
- Terrones, G., Pearlstein, A.J., 2001. Effects of optical attenuation and consumption of a photobleaching initiator on local initiation rates in photopolymerizations. *Macromolecules* 34 (10), 3195.
- Tobolsky, A.V., 1960. *Properties and Structures of Polymers*. Wiley, New York.
- Tobushi, H., Hara, H., Yamada, E., Hayashi, S., 1996. Thermomechanical properties in a thin film of shape memory polymer of polyurethane series. *Smart Materials and Structures* 5 (4), 483.
- Treloar, L.R.G., 1958. *The Physics of Rubber Elasticity*. Clarendon Press, Oxford.
- Warner, M., Terentjev, E.M., 2003. *Liquid Crystal Elastomers*. Oxford University Press, Oxford.
- Wineman, A., Min, J.-H., 2003. Time dependent scission and crosslinking in an elastomeric cylinder undergoing circular shear and heat conduction. *International Journal of Non-Linear Mechanics* 38 (7), 969.
- Wineman, A., Shaw, J., 2004. A correspondence principle for scission-induced stress relaxation in elastomeric components. *Journal of Applied Mechanics, Transactions of the ASME* 71 (6), 769.
- Yakacki, C.M., Shandas, R., Lanning, C., Rech, B., Eckstein, A., Gall, K., 2007. Unconstrained recovery characterization of shape-memory polymer networks for cardiovascular applications. *Biomaterials* 28 (14), 2255.